

1 **Array-wide Uniform PEDOT:PSS Electroplating from Potentiostatic Deposition**

2
3 *Yieljae Shin ^a, Jaehyeon Ryu ^a, Tianyu Bai ^a, Yi Qiang ^a, Yongli Qi ^a, Gen Li ^a, Yunxiang*
4 *Huang ^a, Kyung Jin Seo ^b*, Hui Fang ^a**

5
6
7 ^a Thayer School of Engineering, Dartmouth College, Hanover, NH, 03755, USA

8 ^b Science Corporation, Alameda, CA, 94501, USA

9
10
11 **To whom correspondence should be addressed.*

12 *Hui Fang*

13 *Email: hui.fang@dartmouth.edu*

14 *Tel : (603)646-8656*

15
16 *Kyung Jin Seo*

17 *Email: kjseo22@gmail.com*

18 *Tel : (617)831-5678*

19
20
21
22

1 **Abstract**
2 Electroplating of poly(3,4-ethylenedioxythiophene) polystyrene sulfonate (PEDOT:PSS) is
3 important in many neuroelectronic applications but is challenging to achieve uniformly on
4 large-scale microelectrode arrays (MEA) using conventional galvanostatic methods. In this
5 study, we address this challenge through a potentiostatic method and demonstrate highly
6 uniform electroplating of PEDOT:PSS on MEA with more than one hundred electrodes, all at
7 cellular sizes. The validation of this approach involves comparisons with galvanostatic
8 deposition methods, showcasing unparalleled deposition yield and uniformity. Systematic
9 electrochemical characterizations reveal similarities in structure and stability from
10 potentiostatic deposited coatings. The advances developed here establish the potentiostatic
11 method and detailed process to achieve a uniform coating of PEDOT:PSS on large-scale
12 MEA, with broad utility in neuroelectronics.

13

14 **Keywords**

15 large scale, microelectrode array, PEDOT:PSS, uniformity, potentiostatic

16

17 **1. Introduction**

18 Bioelectricity plays a vital role in the brain (Levin, 2023; Hong and Lieber, 2019) ,
19 possessing rich spatiotemporal dynamic (Townsend and Gong, 2018) that necessitate the use
20 of a large-scale MEA for advanced interfacing (Berdondini et al., 2009). These electrodes
21 facilitate the recording of signals from multiple locations within the targeted tissues (Tian et
22 al., 2023; Chung et al., 2019; Konerding et al., 2018; Lee et al., 2022; Viventi et al., 2011).
23 For instance, the Neuropixel device has been recognized for its capacity to record from
24 thousands of sites, enabling extensive single-unit recordings and brain activity mapping
25 (Steinmetz et al., 2021). Clinical trials involving the Utah array with nearly one hundred
26 microelectrodes have showcased its potential to empower patients in controlling prosthetic
27 devices by neuronal signal interpretation and stimulation (Hochberg et al., 2012).

28 Electrocorticography (ECoG) electrode arrays are instrumental in epilepsy treatment (Xie et
29 al., 2017), and recently, ECoG arrays with hundreds of microelectrodes have enabled speech
30 synthesis by decoding brain signals of spoken sentences(Angrick et al., 2019).

31

32 For microelectrodes, it's imperative to attain a coating of low-impedance materials to
33 ensure high-quality electrode recording (Ludwig et al., 2006; Neto et al., 2018). Several low-
34 impedance coatings, including Iridium Oxide (Cogan et al., 2008), Nanostructured Platinum

1 (Boehler et al., 2015), Platinum-Iridium (Petrossians et al., 2011), Titanium Nitride (Meijs et
2 al., 2015), and PEDOT:PSS (Cui and Zhou, 2007) have been explored. Notably, PEDOT:PSS
3 stands out uniquely due to its exceptional biocompatibility (Miriani et al., 2008),
4 electrochemical property (Wang et al., 2021), and adjustable conductivity (Sanviti et al.,
5 2022) when compared to other materials. ~~The current state of the art approach for~~
6 ~~PEDOT:PSS coating involves galvanostatic electroplating (Pranti et al., 2018; Ji and Wang,~~
7 ~~2020; Qiang et al., 2018), but often requires sequential deposition if there is a large number of~~
8 ~~microelectrodes on the array. Alternative deposition methods, such as spin coating (Cho et al.,~~
9 ~~2021) and sputtering (Hwang et al., 2006) exist; however, for large-scale, high-density~~
10 ~~devices, these techniques may yield non-uniform or non-reliable coatings, potentially~~
11 ~~compromising signal recording accuracy and stability.~~

12 For decades, various deposition methods have been investigated for PEDOT:PSS. For
13 instance, spin coating (Illakkia et al., 2018; Bessaire et al., 2017) could achieve high
14 electrical conductivity and optical transparency with PEDOT-based polymers. However, spin
15 coating is known to be limited to flat substrates and is prone to easier delamination of the
16 film. Inkjet printing is also a recognized method for coating PEDOT-based polymers (Lo et
17 al., 2021), but its effectiveness is contingent upon the physicochemical properties of the ink
18 and requires a longer coating time. Another method is electrospinning, which recently showed
19 PEDOT:PSS nanofiber coating with high electrical conductivity (Bessaire et al., 2017).
20 However, achieving scalability with this methodology still poses challenges. Electroplating is
21 extensively recognized as an effective and reliable method for the deposition of low-
22 impedance materials on microelectrodes, typically utilizing a three-electrode system.
23 Electroplating is further conducted under three modes, namely potentiostatic (constant
24 potential), galvanostatic (constant current), and cyclic voltammetry (voltage sweeping). This
25 method facilitates meticulous regulation of the coating's thickness and composition, offers a
26 straightforward process, and requires minimal deposition time. Additionally, it is adaptable
27 for versatile sample configurations, regardless of their physical forms.

28 While numerous studies have explored the electroplating of PEDOT-based polymers, the
29 exploration of electroplating methods in existing literature often focuses on single electrodes,
30 overlooking the complex dynamics of array-wide deposition essential for MEAs. Studies by
31 Tran et al. (2023), Mousavi et al. (2023) and Teixeira et al. (2022) provide valuable insights
32 into the electrodeposition kinetics and physicochemical characteristics of conducting
33 polymers like PEDOT:PSS. Still, they are conducted on single electrodes or bulk substrates
34 rather than on large-scale MEAs. MEA-level electroplating studies exist, but they usually lack

1 emphasis on electrodes with sizes at the cellular level. For instance, Castagnola et al. (2013),
2 Ji and Wang (2018), and Pranti et al. (2018) have contributed significantly to the field by
3 enhancing the electrochemical properties and biocompatibility of electrode surfaces; however,
4 their investigations predominantly utilized electrodes with sizes orders of magnitude larger
5 than cellular dimensions. This size difference underscores a critical gap, as larger electrode
6 windows compromise spatial resolution, making them less effective for precise neuronal spike
7 detection in highlighting the need for cellular-level electrode precision to enhance signal-to-
8 noise ratio (SNR) (Viswam et al., 2019). Aqrawe et al. (2019) and Jones et al. (2020) have
9 involved smaller electrodes and delved into the intricacies of electrode morphology including
10 complex 3D structures, but a detailed investigation of scalability and uniformity across entire
11 microelectrode arrays during electroplating processes remains missing. This gap hints at an
12 overlooked opportunity to deepen our understanding and innovation in the realm of MEA
13 design and fabrication.

14 To our knowledge, we present the first study focused on (1) array-wide uniform
15 electroplating of PEDOT:PSS on large-throughput (>100 ch) MEAs, with electrode size down
16 to cellular level; (2) comparison of similarities and differences between potentiostatic and
17 galvanostatic electroplating methods in the deposition PEDOT:PSS on large-scale MEAs; (3)
18 understanding of the electrochemical origin of the array-wide uniformity and better scalability
19 from potentiostatic electroplating method. By addressing all the key points highlighted above,
20 our study aims to significantly advance the understanding and application of electroplating in
21 MEAs.

22 To address the uniformity challenges encountered during the deposition of PEDOT:PSS
23 onto large scale MEA, here we demonstrated a potentiostatic electroplating technique for
24 parallel coating of this material uniformly on arrays of up to 128 microelectrodes. We
25 conducted a comparative analysis between the potentiostatic and galvanostatic methods. Our
26 evaluation revealed the potentiostatic method exhibited highly efficient deposition with
27 significantly smaller deviations across microelectrodes than the conventional galvanostatic
28 deposition. Electrochemical impedance spectroscopy (EIS) and cyclic voltammetry (CV)
29 analyses of single electrodes revealed potentiostatic deposited PEDOT:PSS showed
30 electrochemical properties similar to galvanostatic deposited coating. Lastly, we evaluated the
31 chronic stability of PEDOT:PSS deposited using potentiostatic methods through accelerated
32 aging tests. The results indicated impedance remained consistent over a 9 day period at 67 °C,
33 equivalent to 72 days at 37 °C. This research suggests that the potentiostatic deposition of

1 ~~PEDOT:PSS holds promise for neuroelectronics, particularly for large-scale device~~
2 ~~applications.~~

3

4 **2. Materials and Methods**

5 *2.1 Device fabrication*

6 To fabricate the substrate, 3×2 inch² glass was cleaned and blow-dried.
7 Polydimethylsiloxane (PDMS, 10:1 ratio) was spin-coated and cured at 90 °C. Kapton (1 mil
8 thick, Fralock) was laminated, and polyimide (PI 2545, HD MicroSystems) was spin-coated
9 (2 µm thick), cured at 110 °C for 3 minutes, 150 °C for 5 minutes, and 250 °C for 70 minutes.
10 Metals (Cr: 5 nm, Au: 100 nm thick) were deposited via a thermal evaporator. After
11 deposition, micropatterning was done by photolithography (M400, Midas Systems) using
12 positive photoresist (PR, S1805 G2, MicroChem). Negative PR was spin-coated and patterned
13 as an encapsulation layer (SU-8 2005, Kayaku) and hard baked at 180 °C for 30 min. A laser
14 cutter (U4, LPKF) defined outline of the sample, then the device was peeled off from the
15 PDMS layer.

16

17 *2.2 Electrochemical deposition of PEDOT:PSS*

18 DI water (100 ml) was mixed with 3,4-Ethylenedioxythiophene (EDOT) monomer (0.1 %
19 (w/v) 0.01 M, Sigma Aldrich) and poly(sodium-4-styrene sulfonate) powder (PSSNa, (0.7 %
20 (w/v), Sigma Aldrich) to make precursors. After 3 hours of mixing with a magnetic stirrer, the
21 beaker was left in ambient air for an hour to settle down the precipitates. Silver paste (Ted
22 Pella) was pasted gently on the pad area and dried. The copper tape was taped on the edge to
23 have good contact with the potentiostat. Before soaking the device into the solution, gentle O₂
24 plasma (100 W, 1 min) treated the device to have improved water wettability, then connected
25 to a three-electrode system with a potentiostat (Reference 620, Gamry), using a platinum wire
26 (0.5 mm diameter, Sigma Aldrich) as the counter electrode (CE) and an Ag/AgCl reference
27 electrode (RE). Potentiostatic function was used for electroplating PEDOT:PSS with a certain
28 amount of time. After deposition, the device was rinsed and blow-dried, removing excess
29 silver paste and copper tape by swabbing in acetone bath.

30

31 *2.3 Sample assembly*

32 In-house fabricated printed circuit boards (PCB) were used to connect the Intan head stage
33 (RHS 32 ch, Intan technologies) to the electrodes. The device pads were aligned to the PCB
34 solder balls and assembled in a fixed position by sandwiching with soft silicone polymers

1 (Ecoflex 0020, Smooth-on) and an acylate top board. Screws and nuts were assembled to
2 secure the location on every corner of the top board. The PCB is soldered with 32 channel
3 connectors (A79022-001, Omnetics), which could be assembled with the head stage later to
4 measure the device impedances.

5

6 *2.4 Surface Analysis*

7 Digital Optical microscope (VHX-7000N, Keyence) was used to take sample images and
8 check uniformities across the whole sample. Scanning electron miscocopy (SEM, (Thermo
9 Fisher Scientific, Helios 5 CX DualBeam) was used to take the sample surface morphology
10 by using secondary electron (SE) mode. To measure the array impedances, Intan RHS
11 (Stim/Recording system, Intan technologies) was used. For single-electrode Electrochemical
12 impedance spectroscopy (EIS) measurement, potentiostat (Reference 620, Gamry) was used
13 with a 3-electrode system, and the result was analyzed by software (Framework, Gamry).
14 Origin Pro software was used to generate graphs and heatmaps.

15

16 *2.5 Accelerated aging test*

17 PEDOT:PSS samples were prepared and soaked in phosphate-buffered saline (PBS). After
18 positioning, the beaker containing PBS was sealed with Kapton film (0.25 mil thick,
19 Durafilm). The beaker was put in the oven and kept at 67 °C. After soaking, the sample was
20 taken out and cooled down to ambient temperature. After cooling down, the sample was taken
21 out from the beaker and rinsed with DI water. The sample was then reassembled with a PCB,
22 and impedance was measured.

23

24 **3. Result and discussion**

25 *3.1. MEA preparation and PEDOT:PSS deposition*

26 We fabricated arrays of 16, 64, and 128 microelectrodes (electrode pitch of 400 μm) and
27 performed PEDOT:PSS deposition using potentiostatic electroplating. Each electrode opening
28 size was set to $10 \times 20 \mu\text{m}^2$ for this study. Potentiostatic deposition was conducted by applying
29 a constant potential (with reference to a standard Ag/AgCl electrode) to all microelectrodes on
30 a given array, where we temporarily short all contact pads by acetone-removable silver paste.
31 We have determined the specific potential to be the optimal condition through prior
32 experimentation. ~~Notably, potentials below 0.8 V yielded unsatisfactory deposition outcomes.~~
33 ~~At 0.8 V, only a minimal deposition was observed, suggesting that an extended duration~~
34 ~~would be required to achieve a resistance of 100 $\text{k}\Omega$ or less at 1 kHz. Conversely, at 0.9 V, the~~

1 deposition process exhibited an accelerated rate, proving challenging to control (Fig. S1).
2 Within approximately 20 s, deposition was observed extending beyond the designated surface,
3 prone to easy detachment. Consequently, the potential of 0.85 V was chosen as the optimal
4 parameter. This potential not only facilitated ease of control but also allowed for the visual
5 monitoring of deposition progress over a reasonable time. Furthermore, the Au oxidation
6 potential we observed is slightly above 0.9 V and peaked at 1.2 V. Under this condition, 0.85
7 V for PEDOT:PSS is below the threshold for gold oxidation and exhibits optimal deposition
8 control. 0.85 V potential was selected to finely tune the electroplating deposition rate, which
9 is presumably crucial for the coating's morphology and adhesion. This decision was guided
10 by our observations that at 0.8 V, marking the onset of EDOT oxidation and polymerization
11 on the working electrode (Marzocchi et al., 2015; Teixeira et al., 2022), the deposition rate
12 was minimal. Conversely, at 0.9 V, the deposition rate became excessively high, making it
13 challenging to control the rate of deposition effectively. Optical microscopic images for both
14 conditions are shown in Fig. S1.

15

16 Fig. 1 visualizes the method of potentiostatic deposition of PEDOT:PSS on a large-scale
17 MEA and comparison between potentiostatic and galvanostatic methods, depicting the
18 electroplating method of PEDOT:PSS via 3-electrode system, which enables comprehensive
19 deposition across the entire set of electrodes (Fig. 1a). Fig. 1 visualizes PEDOT:PSS
20 electroplating methods on a large-scale MEA, compares potentiostatic and galvanostatic
21 approaches, and assesses their scalability. Fig. 1a presents a schematic representation of the
22 electroplating process for PEDOT:PSS on microelectrode arrays (MEAs) using a three-
23 electrode system. Here, two representative modes for electroplating were illustrated. In
24 potentiostatic deposition, constant potential difference between WE and RE is controlled.
25 Conversely, galvanostatic deposition pivots on the control of current, ensuring a steady
26 current flow between the WE and CE. To highlight the advantage of the potentiostatic
27 deposition approach, we compared the potentiostatic and galvanostatic methods with 128-ch
28 arrays of the same design (Fig. 1b-df). In Fig. 1b, an optical microscopic image of 128-ch
29 (32×4 matrix) is exhibited along with the images of electrodes on every 10th column. The
30 potentiostatic deposition was carried out at 0.85 V and for 20 s, while the galvanostatic
31 method used a 0.2 mA/cm² current density, a typical value for PEDOT:PSS coating on
32 microelectrodes (Qiang et al., 2018). To compare these two methods fairly, we controlled the
33 deposition charge density to be the same. Here, while potentiostatic samples showed
34 electrodes with very similar colors of PEDOT:PSS for all electrodes, the galvanostatic

1 samples did not show uniform coatings. As a result, the average impedance of the
2 microelectrodes from these two methods is similar after the deposition, achieving ~ 100 k Ω
3 and ~ 120 k Ω , respectively, for the potentiostatic and galvanostatic methods. However, the
4 galvanostatic deposited microelectrodes are much less uniform. The standard deviation values
5 were 29.8 k Ω and 168.29 k Ω , for potentiostatic and galvanostatic methods, respectively,
6 showing $\sim 5.5\times$ difference. Furthermore, there are many electrodes with impedances over 600
7 k Ω , which is not suitable for high-performance neural interfacing. Therefore, potentiostatic
8 methods achieve much better uniformity for large-scale MEA. To add statistical powers, we
9 tested more samples (n=4) for each condition (Fig. 1f). As a result, their average mean-
10 impedances were similar (104.31 k Ω and 94.95 k Ω for potentiostatic and galvanostatic
11 deposition, respectively), yet the standard deviation values were notably different (6.39 k Ω
12 and 43.18 k Ω , respectively). This result implies that although the amount of deposition was
13 similar, there was a significant difference in uniformity. Lastly, the scalability test was
14 conducted using MEAs with electrode window sizes of 5 \times 5, 5 \times 10, and 10 \times 10 μm^2 (Fig. 1g-h)
15 for both deposition methods. All samples prepared using potentiostatic deposition were
16 processed under the conditions of 0.85 V for a 20-second deposition time. Conversely,
17 samples created through galvanostatic deposition were ensured to get the same charge density.
18 Potentiostatic deposition demonstrated superior uniformity, achieving a 100% deposition
19 yield (percentage of electrodes successfully coated, cut-off impedance of electrode at 1 kHz:
20 500 k Ω) and an average impedance of 132.45 k Ω with a standard deviation of 23.64 k Ω at
21 5 \times 5 μm^2 . Conversely, galvanostatic deposition at the same size showed less uniformity
22 (deposition yield: 37.5 %), with an average impedance of 172.65 k Ω and a higher standard
23 deviation of 100.74 k Ω , indicating non-uniform coating of PEDOT:PSS. This indication was
24 further vindicated by optical microscopic images (Fig. S2). These results highlight
25 potentiostatic deposition's effectiveness for extremely scaled microelectrodes, essential for
26 high-density neuroelectronic interfaces. Note that for Fig 1. b-h, all impedance values were
27 collected at 1-kHz-frequency.

28
29 ~~This significant difference in uniformity likely arises from the fact that the deposition rate of~~
30 ~~PEDOT:PSS across all microelectrodes on an array is primarily dominated by the~~
31 ~~polymerization reaction rate. From an energetic perspective, the reaction rate is related to the~~
32 ~~electron energy at the electrode, which is determined by its electrical potential. For the~~
33 ~~potentiostatic method, the electrode potential is set to be equal by the potentiostat among all~~
34 ~~microelectrodes, with negligible voltage dividing effect from parasitic resistances such as~~

1 from the interconnect of each microelectrode and the distance between the microelectrode to
2 the CE. On the other hand, in the galvanostatic method, the electrode potential is not
3 controlled among different microelectrodes and can be different from electrode to electrode
4 due to their impedance variations, resulting in different deposition rates across electrodes.

5 To understand the difference between the two methods in depth, we examined the
6 fundamental principles underlying the coating process in electroplating. To start with, we
7 elaborate on the oxidation process of EDOT monomers and the deposition mechanism. The
8 electroplating process initiates with the oxidation of EDOT monomers at the working
9 electrode under a specifically applied voltage. This oxidation results in the formation of two
10 activated monomers that subsequently react, release protons, and generate positively charged
11 PEDOT chains. The negatively charged PSS ions crosslink with these PEDOT⁺ chains,
12 creating an electrostatically stable bipolymer film, as outlined by Mousavi et al. (2023). For
13 potentiostatic deposition, in addressing the optimal conditions for voltage application during
14 electroplating, our research leveraged the Butler-Volmer equation (1), which correlates the
15 electrical current during electroplating with the applied voltage on the electrode.

$$16 \quad j = j_0 \cdot \left\{ \exp \left[\frac{\alpha_a zF}{RT} (V - V_{eq}) \right] - \exp \left[-\frac{\alpha_c zF}{RT} (V - V_{eq}) \right] \right\} \quad (1)$$

17 Here, j is a current density, j_0 is an exchange current density, which reflects the rate of an
18 electrochemical reaction at equilibrium when the activation overpotential ($V - V_{eq}$) is 0. V is an
19 applied potential, whereas V_{eq} is an equilibrium potential. α_c is a cathodic charge transfer
20 coefficient and α_a is an anodic charge transfer coefficient which is a value of $1 - \alpha_a$. z is the
21 number of electrons involved in the electrode reaction, F is the Faraday constant, and R is the
22 universal gas constant. This equation considers both anodic and cathodic reactions in one
23 electrode, and total current density is a sum of currents from both anodic and cathodic
24 reactions. At the low overpotential region, where the applied potential is close to the V_{eq} , the
25 equation could be simplified to:

$$26 \quad j = j_0 \cdot \frac{zF}{RT} (V - V_{eq}) \quad (2)$$

27 , where a linear relationship of overpotential and current density is formed. On the contrary, in
28 high overpotential region, the Butler-Volmer equation is simplified to the Tafel equation,
29 where the activation overpotential is substituted to:

$$30 \quad V - V_{eq} = \pm A \cdot \log_{10} \left(\frac{j}{j_0} \right) \quad (3)$$

31 , with A as the Tafel slope (E. Katz, 2022). In this region, the current density increases at a
32 much higher rate than that of the linear region, which is called the Tafel region. In both

1 regions, it is clear that the deposition current density is determined only by the electrode
2 potential for a given deposition reaction at a given temperature. Therefore, for the
3 potentiostatic deposition, due to the fact that all microelectrodes are applied with the same
4 potential because of parallel connection via conductive paste on the MEA pad area, the same
5 current density will be flowing through all microelectrodes during electroplating. Assuming
6 all current contributes to the Faradaic reaction, this result will lead to the same deposition rate
7 of PEDOT:PSS films across all microelectrodes (T. Niederhoffer et al., 2023). Therefore,
8 array-wide uniform electroplating of PEDOT:PSS on all microelectrodes is achieved.

9 On the other hand, in galvanostatic deposition, the configuration only controls the total
10 current from the working electrode to the counter electrode. Due to the parallel connection of
11 all microelectrodes, the current density at individual microelectrodes can be different from
12 each other, unlike potentiostatic (Fig. S3). This non-uniform distribution of current density is
13 usually inevitable due to different values of microelectrode impedances across the MEA,
14 possibly originating from electrode-to-electrode variations such as the opening area of
15 electrodes, electrode surface roughness, and interconnect length. Electrodes with higher
16 current density compared to others will deposit PEDOT:PSS faster on their surface. This
17 faster deposition will, in turn, reduce the electrode impedance further and promote more
18 current flow and, hence, deposition, thus creating positive feedback on the deposition.
19 Therefore, in galvanostatic deposition, it would be difficult to achieve deposition uniformity
20 of PEDOT:PSS across the large-scale MEA.

21

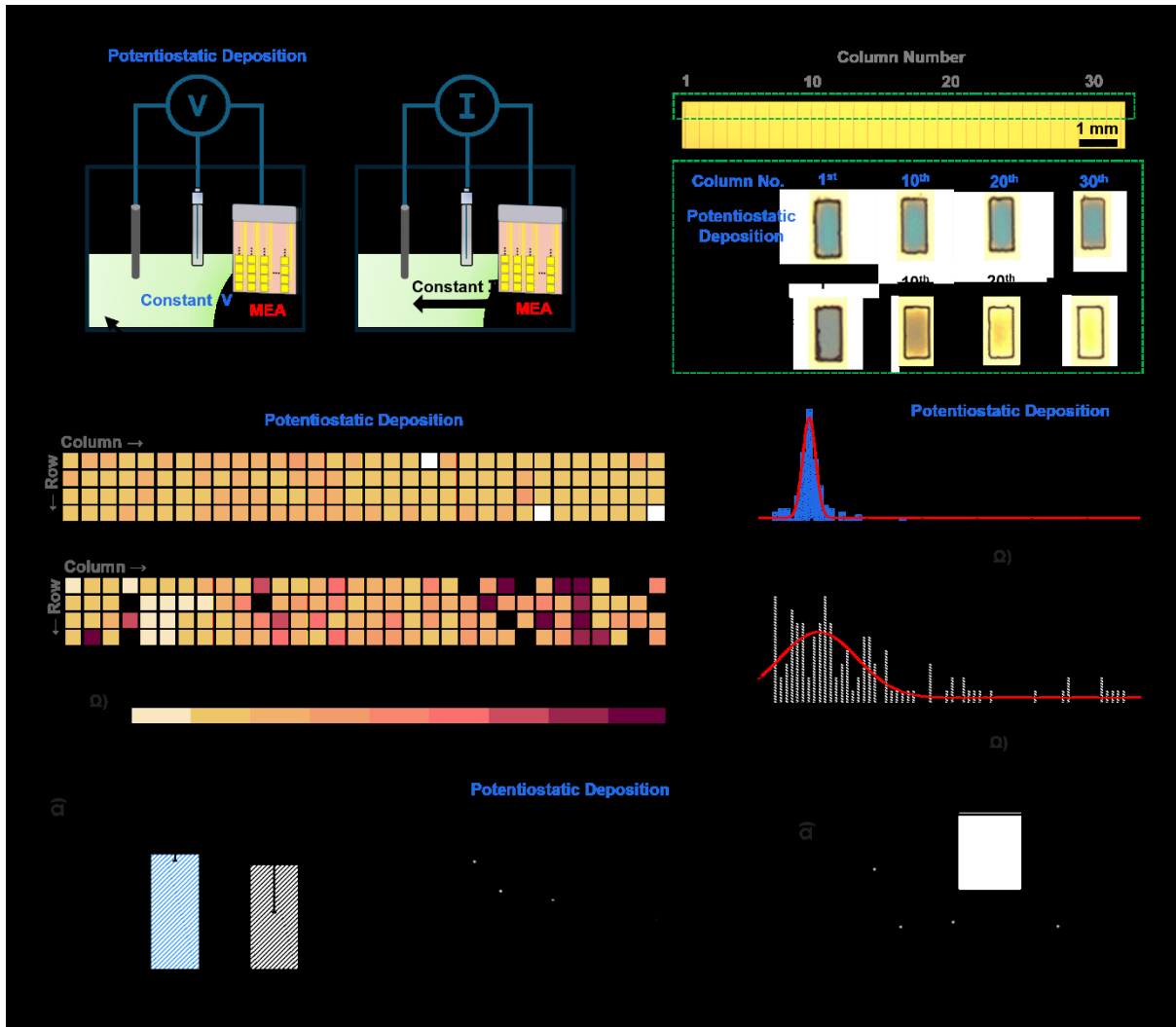
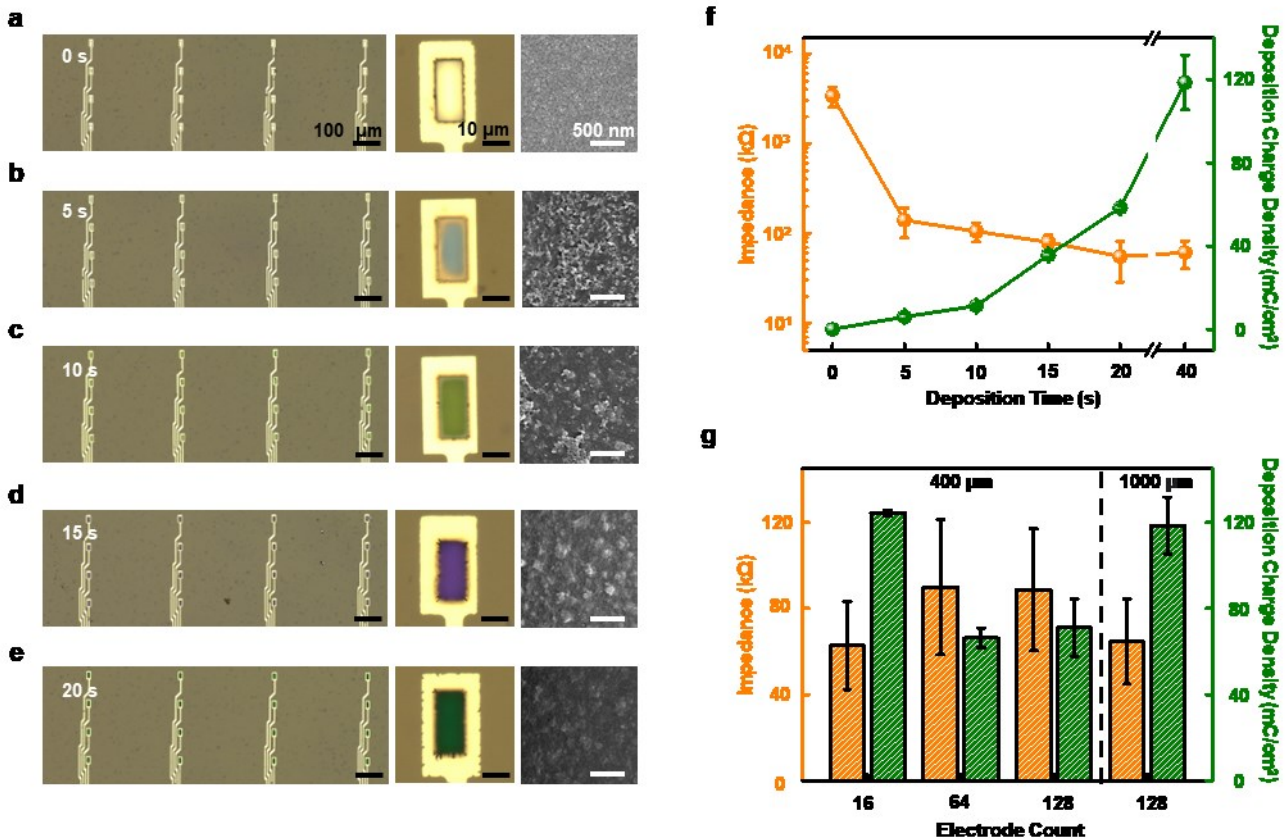


Fig. 1. Demonstration of PEDOT:PSS electroplating on a large-scale MEA and scalability test results. (a) Illustration of PEDOT:PSS electroplating in 3 electrode system and schematics of current density for potentiostatic and galvanostatic deposition in large-scale MEA. (b) Optical microscopic image of 128 ch MEA with magnified images ($\times 400$) of electrodes after electroplating. Electrode area: $10 \times 20 \mu\text{m}^2$. (c) Impedance heatmap for potentiostatic deposition and galvanostatic deposition method. (d) Impedance histogram from potentiostatic deposition. (e) Impedance histogram from galvanostatic deposition. (f) Average mean-impedance of 128 ch MEA based on deposition methods. (g) Impedance and deposition yield (cut-off impedance: $500 \text{ k}\Omega$) over various electrode opening areas in potentiostatic deposition, Electrode area : 5×5 , 5×10 , 10×10 , $10 \times 20 \mu\text{m}^2$. (h) Impedance and deposition yield over various electrode opening areas in galvanostatic deposition.

The electrode uniformity and surface color with respect to deposition time under the aforementioned conditions, accompanied by morphological changes were observed through scanning electron microscopy (SEM) analysis. In all instances, deposition progressed

1 independently, with coating evident in all conditions. Specifically, after 5 s (Fig. 2b),
2 deposition is evident, yet full electrode coverage is not achieved, particularly at the edges.
3 SEM analysis reveals partial exposure of the Au surface, indicating incomplete coating. With
4 a total deposition time of 10 s (Fig. 2c), a complete electrode coating is observed, resulting in
5 an overall color of light green. SEM further confirms uniform deposition across the entire
6 electrode. At a 15 s deposition (Fig. 2d), the coating exhibits a shift in color to purple and
7 further evolves into dark green after an additional 5 s deposition (Fig. 2e), with both
8 microscopic and SEM analyses showing negligible lateral growth of PEDOT:PSS. Overall,
9 the findings here suggest that uniform deposition of PEDOT:PSS on all electrodes is
10 simultaneously achievable with potentiostatic deposition carried out at 0.85 V. Moreover, this
11 deposition process is highly controllable by tuning the deposition time. At 0-s deposition
12 (bare Au electrodes, Fig. 2a), since there was no deposition of PEDOT:PSS, we could only
13 observe the surface of the gold film generated by E-beam evaporation. At 5-s deposition (Fig.
14 2b), deposition is evident, yet full coverage is not achieved. For the 10-s deposition (Fig. 2c),
15 a complete coating is observed, resulting in an overall color of light green. From SEM, we
16 could see that the surface of the electrode is fully covered with PEDOT:PSS. Here,
17 cauliflower-like grains of coating were starting to form. According to V. Castagnola et al.
18 (2014), PEDOT-rich regions are observed to be slightly brighter than other areas, enclosed in
19 insulating PSS-rich shells. In 15-s deposition samples (Fig. 2d), the coating exhibits a shift in
20 color to purple. From SEM, we could observe larger grains compared to 10-s deposition, with
21 brighter images. This implies that the electrical conductivity increased with more deposition,
22 possessing more PEDOT-rich morphologies. In the 20-s deposition (Fig. 2e), the color
23 transitioned into dark green. From SEM, the image brightness was lower compared to 15-s
24 deposition. This could be due to the charging effect of polymers, where the surface of
25 polymers becomes less conductive because of excessive deposition even though it is
26 conductive. Therefore, instead of dissipating the charge, it accumulates and shows darker
27 contrast than the sample with previous deposition condition.

28



1
2 **Fig 2. Optical and electrochemical analysis of MEAs with various potentiostatic**
3 **deposition times.** Optical microscopic and SEM images of MEAs with a deposition time of
4 (a) 0 s (bare Au electrodes), scale bar: 100 μ m (left), 10 μ m (middle), 500 nm (right). (b) 5 s.
5 (c) 10 s. (d) 15 s. (e) 20 s. (f) Impedance & total deposition charge over various deposition
6 times for 16-ch electrode arrays (0, 5, 10, 15 and 20 s). (g) Impedance & total deposition
7 charge over various array configurations (16, 64, 128-ch arrays with 400 μ m pitch and 128-ch
8 arrays with 1000 μ m horizontal pitch), deposition condition: 0.85 V, 40 s.

9
10 *3.2 Impedance analysis*
11 From the potentiostatic deposition, it is apparent that the deposition charge increases as a
12 function of increasing deposition time. Fig. 2f presents the impedance values at 1 kHz for a
13 group of 16-ch samples with different amounts of PEDOT:PSS coating, together with the
14 cumulative deposition charge. Before deposition, the bare Au microelectrode exhibits a 1-kHz
15 impedance of approximately 2.5 M Ω for a 200 μ m² site area. With progressing deposition
16 from 5 to 20 s, the impedance decreases progressively from \sim 150 k Ω to \sim 60 k Ω . However,
17 beyond 20 s, there is no tendency for the impedance to experience a significant decrease, as
18 evidenced by remarkably similar values obtained from the 40-s deposition compared to 20 s.
19 Meanwhile, the deposition charge density continues to increase over time. This phenomenon

1 indicates that, despite more coating, saturation is eventually observed in impedance (Dijk et
2 al., 2020).

3

4 We further investigated the effect of the total number of electrodes on the deposition
5 (Fig. 2g). With the same potentiostatic deposition condition, we observed an electrode number
6 effect where the deposition charge density overall decreases with the increasing electrode
7 number, consequently leading 1-kHz-impedance to increase. This effect is presumably due to
8 the reaction-diffusion process in the electroplating, where the diffusion process will be
9 impacted by the electrode number and affect the overall deposition rate. This hypothesis is
10 further validated by the fact that when comparing 128-ch arrays with a 400 and 1,000 μm
11 horizontal pitch, the sample with a 1,000 μm pitch had much lower impedance and higher
12 deposition charge. As the electrode density decreases, the EDOT and PSS precursors can
13 more quickly diffuse onto the microelectrodes, where they are consumed during the
14 polymerization process. Although we have not tested the effects of electrode pitch less than
15 400 μm under the same electrode numbers in galvanostatic deposition, it is speculated that
16 impedance also increases with a decrease in pitch. We expect the same reaction-diffusion
17 competition to happen in galvanostatic deposition when the electrode pitch is reduced. Note in
18 all conditions, uniformity among electrodes was ensured during visual check in the
19 potentiostatic deposition.

20

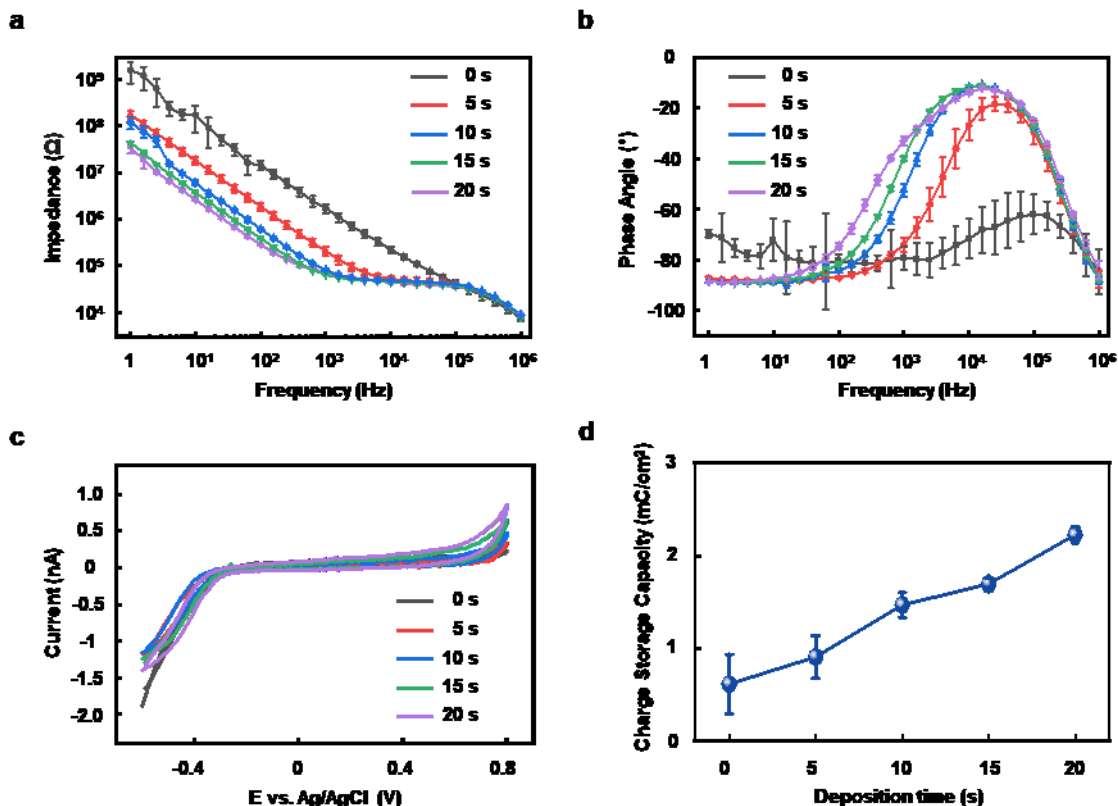
21 *3.3 Single electrode electrochemical characterization*

22 To further analyze the properties of the PEDOT:PSS coating from potentiostatic
23 electroplating, EIS and CV measurements were performed from 1 Hz to 1 MHz using a three-
24 electrode setup with a potentiostat (n=4). As expected, the impedance decreased significantly
25 as a function of the PEDOT:PSS deposition time, especially between 1 Hz – 1 kHz (Fig. 3a).
26 The trend of impedance decrease again slowed down with further deposition, which is
27 consistent with previous observations (Fig. 3a, S42) From the phase spectra perspective, for
28 the frequency below 1 kHz, the phase angle is $\sim -90^\circ$ for all PEDOT:PSS coated cases (Fig.
29 3b). This phenomenon implies that for this region, the electrode behaves mostly capacitive,
30 and impedance is dominated by the capacitive coupling of the material (Wang et al., 2021).
31 However, at higher frequencies, phase angle value decreases, and this effect is more
32 prominent with longer PEDOT:PSS deposition time. This phase angle change is due to the
33 efficient charge transfer at the PEDOT:PSS-electrolyte interface, lowering the charge transfer
34 resistance. We also prepared and analyzed the EIS of the single electrode sample with the

1 galvanostatic method (Fig. S35). Overall, there is no qualitative difference in impedance or
 2 phase spectra comparing the potentiostatic with galvanostatic depositions, indicating similar
 3 PEDOT:PSS structures from these two methods. This similarity is not unexpected since the
 4 overall methodology of coating is the same electroplating for the two methods.

5
 6 We also performed CV measurement, scanning between -0.6 V and 0.8 V, with a scan rate
 7 of 50 mV/s. As shown in Fig. 3c, PEDOT:PSS deposition onto the Au microelectrode
 8 increased its charge storage capacity (CSC), evidenced by the broader enclosed area of the
 9 CV curve. This CSC increase continued with more PEDOT:PSS was deposition, reaching ~
 10 2.2 mC/cm² at 20-s deposition (Fig. 3d). PEDOT:PSS coating tends to have micro- and nano-
 11 porous structures, increasing its effective surface area with increasing thickness. For
 12 galvanostatic method samples, the CSC value reached ~ 1.35 mC/cm², which is between 5-
 13 and 10-s samples of the potentiostatic method. However, the CSC standard deviation of
 14 multiple samples from the galvanostatic method is larger (~0.32 mC/cm²) compared to that of
 15 from the potentiostatic method (0.23 and 0.13 mC/cm² for 5- and 10-s samples, respectively)
 16 due to bigger sample-to-sample variation from the galvanostatic method.

17



18

1 **Fig. 3. Single electrode electrochemical characterization as a function of various**
2 **deposition times (0, 5, 10, 15and 20 s).** (a) Bode plot of impedance. (b) Bode plot of phase
3 angle. (c) CV. (d) CSC.

4

5 *3.4 Chronic stability tests*

6 For many microelectrode applications, chronic stability is important to ensure stable
7 recording and stimulation performance. To this end, we prepared arrays of microelectrodes
8 with potentiostatic PEDOT:PSS deposition and soaked them in PBS to monitor their
9 impedance and yield changes (Fig. 4). We define yield as a percentage of the number of
10 electrodes with measured impedance that does not exceed the cut-off values out of the total
11 number of electrodes. We set the value of the cut-off impedance as $500\text{ k}\Omega$, a typical value in
12 neuroelectronic applications (Park et al., 2014). To accelerate the aging tests, the soaking
13 temperature was set as $67\text{ }^\circ\text{C}$, offering an acceleration factor of 8 compared to $37\text{ }^\circ\text{C}$,
14 assuming an accelerated aging factor Q_{10} of 2 (Hukins et al., 2008). Fig. 4a shows the images
15 of the same electrode by days of soaking, from day 0 to day 9. Here, we used 15-s deposition
16 condition for chronic stability evaluation since this showed the most promising
17 electrochemical performance. More accelerated aging test results are described in Fig. S46
18 and S57. Through the optical microscope, we observed no delamination or other damage to
19 PEDOT:PSS coating over time, as well as no significant change in the color. For the adhesion
20 performance, we compared our results with other research results. Qiang et al. (2018)
21 performed a chronic soak test for 5 weeks in $37\text{ }^\circ\text{C}$ PBS, while we demonstrated that we could
22 achieve 8 days in PBS, $67\text{ }^\circ\text{C}$, which is equivalent to 72 days in $37\text{ }^\circ\text{C}$ with near 100 %
23 adhesion of the film. Furthermore, our results are similar to Luo et al. (2011) where they
24 performed chronic soaking of the film for 3 months at $37\text{ }^\circ\text{C}$ with PEDOT/CNT. Therefore, it
25 is evident that our adhesion is comparable with studies conducted so far. These observations
26 are consistent with the impedance and yield trends, where both the impedance and array yield
27 remained highly stable over the entire soak duration (Fig. 4b). This stability of 9 days at $67\text{ }^\circ\text{C}$
28 is equivalent to 72 days at $37\text{ }^\circ\text{C}$, suggesting that potentiostatic coated PEDOT:PSS is
29 promising for chronic applications.

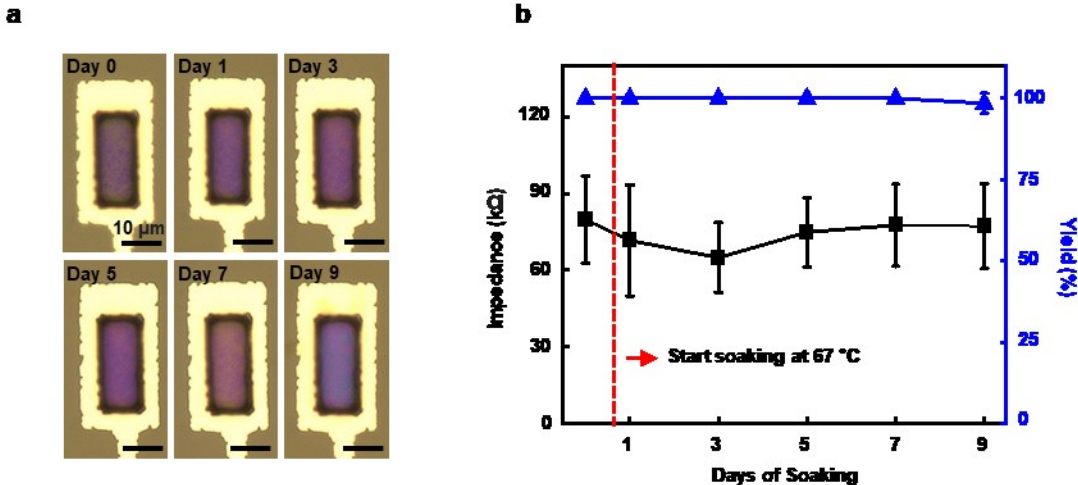


Fig. 4. Chronic stability of PEDOT:PSS with potentiostatic deposition. (a) Optical microscopic images of PEDOT:PSS with 15-s deposition time at different soaking days at 67 °C (scale bar: 10 μ m). (b) 1-kHz electrode impedance and array yield (cut-off impedance: 500 k Ω) as a function of soaking days.

4. Conclusion

In summary, we successfully demonstrated array-wide uniform coating of PEDOT:PSS on arrays of up to 128 microelectrodes using the potentiostatic deposition method. Time-dependent studies revealed that this deposition process is highly controllable, with rates dependent on the electrode throughput and density. In this study, we have successfully demonstrated (1) the capability of achieving array-wide uniform electroplating of PEDOT:PSS on large-throughput (>100 channels) microelectrode arrays (MEAs) with electrode sizes downscaled to the cellular level; (2) a detailed comparison that elucidates the similarities and differences between potentiostatic and galvanostatic electroplating methods in depositing PEDOT:PSS on large-scale MEAs; and (3) a deeper understanding of the electrochemical origins that underlie the array-wide uniformity and enhanced scalability offered by the potentiostatic electroplating method. Through ~~FROM~~ EIS and CV analyses, we found that there was no significant difference in PEDOT:PSS electrochemical properties between the two methods, although galvanostatic deposition samples led to a larger sample-to-sample deviation. Lastly, accelerated aging tests in PBS revealed that PEDOT:PSS from the potentiostatic coating was stable for 9 days at 67 °C. Overall, our study established potentiostatic electroplating as a new coating method for large-scale MEA to achieve uniform PEDOT:PSS coating, with broad applications in bioelectronics. We envision facilitating our

1 novel electroplating method to enable the electroplating of large-scale MEA, surpassing a
2 count of 1,000 channels, with the goal of expanding its application to active devices.
3

4 **Acknowledgments**

5 ~~Y. Shin and J. Ryu contributed equally to this work.~~ The authors acknowledge support from
6 the National Institutes of Health grant U01NS123668 and RF1NS118301, the National
7 Science Foundation grant 2140392, and the Dartmouth College institutional fund.
8

9 **References**

10 M. Levin, 2023. Bioelectric networks: the cognitive glue enabling evolutionary scaling
11 from physiology to mind, *Anim. Cogn.* 26, 1865–1891.

12 G. Hong, C.M. Lieber, 2019. Novel electrode technologies for neural recordings, *Nat. Rev.*
13 *Neurosci.* 20, 330-345.

14 R. G. Townsend, P. Gong, 2018. Detection and analysis of spatiotemporal patterns in brain
15 activity, *PLoS Comput. Biol.* 14, e1006643.

16 L. Berdondini, K. Imfeld, A. Maccione, M. Tedesco, S. Neukom, M. Koudelka-Hep, S.
17 Martinoia, 2009. Active pixel sensor array for high spatio-temporal resolution
18 electrophysiological recordings from single cell to large scale neuronal networks, *Lab Chip* 9,
19 2644-2651.

20 Y. Tian, J. Yin, C. Wang, Z. He, J. Xie, X. Feng, Y. Zhou, T. Ma, Y. Xie, X. Li, T. Yang,
21 C. Ren, C. Li, Z. Zhao, 2023. An Ultraflexible Electrode Array for Large-Scale Chronic
22 Recording in the Nonhuman Primate Brain, *Adv. Sci.* 10, 2302333.

23 J. Chung, H. R. Joo, J. L. Fan, D. F. Liu, A. H. Barnett, S. Chen, C. Geaghan-Breiner, M.
24 Karlsson, M. Karlsson, K. Y. Lee, H. Liang, J. F. Magland, J. A. Pebbles, A. Tooker, L.
25 Greengard, V. Tolosa, L. M. Frank, 2019. High-Density, Long-Lasting, and Multi-region
26 Electrophysiological Recordings Using Polymer Electrode Arrays, *Neuron* 101, 21-31.

27 W. Konerding, U. P. Froriep, A. Kral, P. Baumhoff, 2018. New thin-film surface electrode
28 array enables brain mapping with high spatial acuity in rodents, *Sci. Rep.* 8, 3825.

29 J. Y. Lee, S. H. Park, Y. Kim, Y. U. Cho, J. Park, J.-H. Hong, K. Kim, J. Shin, J. E. Ju, I. S.
30 Min, M. Sang, H. Shin, U. Jeong, Y. Gao, B. Li, A. Zhumbayeva, K. Y. Kim, E.-B. Hong, M.
31 Nam, H. Jeon, Y. Jung, H. Cheng, I. Cho, K. J. Yu, 2022. Foldable three dimensional neural
32 electrode arrays for simultaneous brain interfacing of cortical surface and intracortical
33 multilayers, *npj Flex. Electron.* 6, 86.

1 J. Viventi, D. Kim, L. Vigeland, É. Fréchette, J. A. Blanco, Y.-S. Kim, A. E. Avrin, V.
2 Tiruvadi, S. W. Hwang, A. C. Vanleer, D. Wulsin, K. A. Davis, C. E. Gelber, L. A. Palmer, J.
3 Van Der Spiegel, J. Wu, J. Xiao, Y. Huang, D. Contreras, J. A. Rogers, B. Litt, 2011.
4 Flexible, foldable, actively multiplexed, high-density electrode array for mapping brain
5 activity in vivo, *Nat. Neurosci.* 14, 1599-1605.

6 N. A. Steinmetz, Ç. Aydin, A. Ю. Лебедева, M. Okun, M. Pachitariu, M. Bauža, M. Beau,
7 J. Bhagat, C. Böhm, M. Broux, S. Chen, J. Colonell, R. J. Gardner, B. Karsh, F. Kloosterman,
8 D. Kostadinov, C. M. López, J. O'Callaghan, J. Park, J. Putzeys, B. Sauerbrei, R. Van Daal,
9 A. Z. Volland, S. Wang, M. Welkenhuysen, Y. Z, J. T. Dudman, B. Dutta, A. W. Hantman, K.
10 D. M. Harris, A. K. Lee, E. I. Moser, J. O'Keefe, A. Renart, K. Svoboda, M. Häusser, S.
11 Haesler, M. Carandini, T. D. Harris, 2021. Neuropixels 2.0: A miniaturized high-density
12 probe for stable, long-term brain recordings, *Science* 372, eabf4588.

13 L. R. Hochberg, D. Bacher, B. Jarosiewicz, N. Y. Masse, J. D. Simeral, J. Vogel, S.
14 Haddadin, J. Liu, S. S. Cash, P. Van Der Smagt, J. P. Donoghue, 2012. Reach and grasp by
15 people with tetraplegia using a neurally controlled robotic arm, *Nature* 485, 372-375.

16 K. Xie, S. Zhang, S. Dong, S. Li, C. Yu, K. Xu, W. Chen, W. Guo, J. Luo, Z. Wu, 2017.
17 Portable wireless electrocorticography system with a flexible microelectrodes array for
18 epilepsy treatment, *Sci. Rep.* 7, 7808.

19 M. Angrick, C. Herff, E. M. Mugler, M. C. Tate, M. W. Slutsky, D. J. Krusinski, T.
20 Schultz, 2019. Speech synthesis from ECoG using densely connected 3D convolutional neural
21 networks, *J. Neural Eng.* 16, 036019.

22 K. A. Ludwig, J. D. Uram, J. Yang, D. C. Martin, D. R. Kipke, 2006. Chronic neural
23 recordings using silicon microelectrode arrays electrochemically deposited with a poly(3,4-
24 ethylenedioxythiophene) (PEDOT) film, *J. Neural Eng.* 3, 59.

25 J. P. Neto, P. Baião, G. Lopes, J. Frazão, J. Nogueira, E. Fortunato, P. Barquinha, A. R.
26 Kampff, 2018. Does Impedance Matter When Recording Spikes With Polytrodes?, *Front.*
27 *Neurosci.* 12.

28 S. F. Cogan, J. Ehrlich, T. D. Plante, A. Smirnov, D. B. Shire, M. D. Gingerich, J. F. Rizzo,
29 2008. Sputtered iridium oxide films for neural stimulation electrodes, *J. Biomed. Mater. Res.*
30 *Part B Appl. Biomater.* 89B, 353-361.

31 C. Boehler, T. Stieglitz, M. Asplund, 2015. Nanostructured platinum grass enables superior
32 impedance reduction for neural microelectrodes, *Biomaterials* 67, 346-353.

1 A. Petrossians, J. J. Whalen III, J. D. Weiland, F. Mansfeld, 2011. Electrodeposition and
2 Characterization of Thin-Film Platinum-Iridium Alloys for Biological Interfaces,
3 J. Electrochem. Soc. 158, D269.

4 S. Meijs, M. V. Fjorback, C. Jensen, S. Sørensen, K. Rechendorff, N. Rijkhoff, 2015.
5 Electrochemical properties of titanium nitride nerve stimulation electrodes: an in vitro and in
6 vivo study, Front. Neurosci. 9.

7 X. T. Cui, D. D. Zhou, 2007. Poly (3,4-Ethylenedioxothiophene) for Chronic Neural
8 Stimulation, IEEE Trans. Neural Syst. Rehabil. Eng. 15, 502-508.

9 R. M. Miriani, M. R. Abidian, D. R. Kipke, 2008. Cytotoxic analysis of the conducting
10 polymer PEDOT using myocytes, Annual Int. Conf. of the IEEE, 1841-1844.

11 A. Wang, D. Jung, D. Lee, H. Wang, 2021. Impedance Characterization and Modeling of
12 Subcellular to Micro-sized Electrodes with Varying Materials and PEDOT:PSS Coating for
13 Bioelectrical Interfaces, ACS Appl. Mater. 3, 5226-5239.

14 M. Sanviti, D. E. Martínez-Tong, E. Rebollar, T. A. Ezquerra, M. C. García-Gutiérrez,
15 2022. Crystallization and phase separation in PEDOT:PSS/PEO blend thin films: Influence on
16 mechanical and electrical properties at the nanoscale, Polymer 262, 125475.

17 A. S. Pranti, A. Schander, A. Bödecker, W. Lang, 2018. PEDOT: PSS coating on gold
18 microelectrodes with excellent stability and high charge injection capacity for chronic neural
19 interfaces, Sens. Actuators B Chem. 275, 382-393.

20 B. Ji, M. Wang, 2020. Micro-wrinkle strategy for stable soft neural interface with
21 optimized electroplated PEDOT:PSS, J. Micromech. Microeng. 30, 104001.

22 Y. Qiang, P. Artoni, K. J. Seo, S. Culaclii, V. Hogan, X. Zhao, Y. Zhong, X. Han, P. Wang,
23 Y. Lo, Y. Li, H. A. Patel, H. Yifu, A. Sambangi, J. S. V. Chu, W. Liu, M. Fagiolini, H. Fang,
24 2018. Transparent arrays of bilayer-nanomesh microelectrodes for simultaneous
25 electrophysiology and two-photon imaging in the brain, Sci. Adv. 4, eaat0626.

26 Y. U. Cho, J. Y. Lee, U. Jeong, S. H. Park, S. L. Lim, K. Y. Kim, J. W. Jang, J. H. Park, H.
27 W. Kim, H. Shin, H. J. Jeon, Y. M. Jung, I. Cho, K. J. Yu, 2022. Ultra-Low Cost, Facile
28 Fabrication of Transparent Neural Electrode Array for Electrocorticography with
29 Photoelectric Artifact-Free Optogenetics, Adv. Funct. Mater. 32, 2105568.

30 J. Hwang, F. Amy, A. Kahn, 2006. Spectroscopic study on sputtered PEDOT · PSS: Role
31 of surface PSS layer, Org. Electron. 7, 387-396.

32 G. Dijk, H. Ruigrok, R. O'Connor, 2020. Influence of PEDOT:PSS Coating Thickness on
33 the Performance of Stimulation Electrodes, Adv. Mater. Interfaces 7, 2000675.

1 D. W. L. Hukins, A. Mahomed, S. N. Kukureka, 2008. Accelerated aging for testing
2 polymeric biomaterials and medical devices, *Med. Eng. Phys.* 30, 1270-1274.

3

4

5

6

7